RSC Advances

ROYAL SOCIETY OF CHEMISTRY

www.rsc.org/advances

Journal Name

ARTICLE

Synthesis and characterization of a quaternary nanocomposite based on TiO₂/CdS/rGO/Pt and its application in the photoreduction of CO₂ to methane under visible light

[1]J. E. Benedetti, [1]D. R. Bernardo, [1]A. Morais, [2]Jefferson Bettini and [1]A. F. Nogueira

[1]Chemistry Institute, University of Campinas – UNICAMP, P.O. Box 6154, 13083-970, Campinas, SP, Brazil.
[2] National Nanotechnology Laboratory, National Center for Energy and Materials Research, CNPEM, 13083-970, Campinas, São Paulo, Brazil.

'Together we are stronger' In this work, the preparation of the quaternary nanocomposite TiO₂/CdS/rGO/Pt is reported along with its application, for the first time, as a catalyst for the photocatalytic reduction of carbon dioxide (CO_2) to methane (CH_4). TiO₂/CdS nanoparticles and Pt nanoparticle-decorated reduced graphene oxide sheets (rGO/Pt) were synthesized separately and characterized through X-ray diffraction (XRD), scanning electron microscopy (SEM), high-resolution transmission electron microscopy (HR-TEM), Raman spectroscopy, UV-vis spectroscopy and photoelectrochemical experiments. Hydrocarbon samples were collected and analysed using gas chromatography (GC). After 5 hours of illumination under visible light, 0.11 µmol of CH_4 was produced at an average production rate of 0.0867 µmol/hour, which is higher than the production of CH_4 measured from the TiO₂/CdS and the TiO₂/CdS/Pt control samples. The photoelectrochemical experiments confirmed that the presence of rGO sheets in the nanocomposite enhanced the electrochemical and photocatalytic properties of the nanocomposite as a result of rapid electron transport and the inhibition of charge recombination.

Address all correspondence to: Ana Flavia Nogueira, University of Campinas (UNICAMP), Chemistry Institute, Campinas-SP, Brazil, P. O. Box 6154, 13083-970, Tel: +55 19 35213029; Fax: +55 19 35213023; E-mail: anaflavia@iqm.unicamp.br.
*JEB, DRB and AM have contributed equally to this work.

1. Introduction

Considerable attention has been devoted to the consequences resulting from the greenhouse effect, which arises from the increasing concentrations of CO_2 and other harmful gases in the atmosphere [1]. One strategy to minimize this effect is to capture these gases from the atmosphere and convert them into more economically attractive substances. Therefore, capturing and converting carbon dioxide into hydrocarbons has attracted considerable attention in both the scientific community and in industry [2,3]. Several studies on the reduction of CO_2 to methanol (CH_3OH), formaldehyde (HCOOH), and methane (CH_4) [4-17] have been reported. Among the hydrocarbons produced from carbon dioxide, methane is one of the products with economic appeal as a fuel because of its high energy density (55.7 kJ g⁻¹) [8].

Different strategies have been proposed for converting carbon dioxide into hydrocarbons, such as thermochemical[9], electrochemical[10,11] and photoelectrochemical methods[12]. Among the methods applied for this purpose, the photoreduction of CO_2 using water and sunlight is a promising and elegant strategy because it uses the sun as the energy source in a process that is similar to photosynthesis in plants. In general, this process can be performed using suitable semiconductors that are able to absorb visible radiation [13]. When a semiconductor is illuminated with energy greater than or equal to its band gap, electrons (e^-) are promoted from its valence band (VB) to the conduction band (CB) [13,14]. Once within the conduction band, electrons can reduce carbon dioxide to hydrocarbons in the presence of H^+ ions. The positive charges (holes - h^+) remaining in the valence band can oxidize water molecules to oxygen gas, thereby generating protons (H^+).

TiO₂ is typically employed as the semiconductor of choice in studies of photocatalyzis because of its relatively low cost, excellent stability over a broad pH range, corrosion resistance and strong oxidizing power [15]. Nevertheless, its wide band gap allows for the absorption of ultraviolet light, which is a drawback for the application of TiO₂ in photocatalyzis using sunlight as the

illumination source. This drawback can be circumvented by doping TiO_2 with anions or cations, by sensitizing with dyes or by combining with another semiconductor with a narrow band gap that is able to absorb radiation within the visible range [16,17]. Cadmium sulfide (CdS) has been widely used in conjunction with TiO_2 in photocatalytic systems due to its strong absorption in the visible region of the solar spectrum[18,19]. The use of TiO_2/CdS composites provides optical and catalytic properties that differ from those of the individual constituent materials. Depending on the nanoparticle size, CdS provides broad visible light absorption, proper thermal stability and resistance to photodegradation when coated with a protecting layer [20,21].

One of the primary drawbacks in photocatalyzis is the poor conversion efficiency provided by these systems, which is on average 2.5% (quantum efficiency) under visible light [22]. The efficiency values found for these photocatalytic systems are primarily associated with the fast dynamic charge recombination of photogenerated charges (electron-hole)[23,24]. It is largely accepted that the photogenerated electrons in the semiconductor (without any bias voltage from an external source) are conducted through the material by diffusion among the nanoparticles[25,26]. The process of electrons diffusing in the semiconductor is not efficient because of surface defects, which result in an increase in charge recombination processes (e^- with h^+), thereby decreasing the photocatalytic efficiency[24]. An interesting approach to decrease this effect is to improve electron transport in the system by introducing conducting carbonaceous materials. Xia et al.[27] reported that TiO_2 electrodes containing dispersed carbon nanotubes (MWCNTs) are more efficient in the photocatalytic reduction of CO_2 than analogous TiO_2 electrodes without the presence of the carbonaceous material [27,28]. More recently, many researchers have reported increases in the photocatalytic activity of several semiconductors by preparing composites with MWCNTs or graphene-based materials [29-31]. This photocatalytic approach is more efficient than the use of small amounts of metal nanoparticles known as co-catalysts deposited onto the semiconductor surface or onto the surface of carbonaceous materials [32]. Metal nanoparticles commonly used as co-catalysts are Ni, Ti, Co, Rh, Ir and Pt [33]. Pt-based composites are interesting because of their unique properties, and these composites are used in several applications in magnetic, catalytic, and biomedical areas[34]. These nanocomposites are currently considered to be the most effective catalysts for hydrogen evolution [35] and for CO_2 reduction [36], primarily because of their stability, chemical inertness and high catalytic activity.

Hence, this work presents, for the first time, the use of the quaternary nanocomposite TiO_2/CdS/rGO/Pt as a catalyst for the photocatalytic reduction of CO_2 to methane using water and visible light as the only energy sources. Samples of TiO_2/CdS and rGO/Pt were prepared separately and then mixed to obtain TiO_2/CdS/rGO/Pt nanocomposite films. Each individual component and the quaternary nanocomposite were characterized using X-ray diffraction, scanning electron microscopy, electron transmission microscopy, Raman spectroscopy and UV-Vis spectroscopy. The photocatalytic activity of the TiO_2/CdS/rGO/Pt system for the conversion of CO_2 to methane was investigated for five hours using a homemade photoreactor.

2. Experimental section

2.1. Synthesis of TiO_2/CdS nanoparticles

The procedure used for the preparation of TiO_2/CdS nanoparticles was similar to that described by Li et al[37]. First, 1.5 g of the polymer Pluronic® F-127 (BASF) was dissolved in 19 mL of ethanol containing 0.14 g of $Cd(NO_3)_2.4H_2O$. Titanium tetrachloride

(0.015 mol) was then added to this solution, which was vigorously stirred for 1 h. The resulting solution was deposited onto a Petri dish, and the system was maintained at 40 ºC for 4 days under ambient conditions for solvent evaporation. The material was heated at 400 ºC for 4 h (EDG3P – S model, EDG) to produce TiO_2/CdO powder. Then, 0.3 g of TiO_2/CdO powder was dispersed in 50 mL of an aqueous solution containing Na_2S (0.2 mol L^{-1}) at room temperature. After 6 h of continuous stirring, the resulting product was obtained by filtering, washed three times with distilled water and then dried. The semiconductor samples were characterized by X-ray diffraction using a Shimadzu –XDR 7000 diffractometer equipped with a copper tube and a graphite monochromator and operated at a power of 40 kV and 35 mA. Scanning electron microscopy images were acquired using a FEI Inspect F50 – High-Resolution SEM operated at a voltage of 5 to 10 kV and current of 12 µA. High-resolution transmission electron microscopy images were acquired using a HRTEM-JEM 3010 URP microscope. Raman spectra were recorded using a Raman confocal spectrometer, model T64000 - Jobin Yvon – USA, with an exposure time of 30 s, accumulation of 10 spectra and laser excitation of 514.5 nm in the frequency range of 200-800 cm^{-1}.

2.2. Synthesis of platinum nanoparticles on graphene oxide

The deposition of Pt nanoparticles onto graphene oxide sheets was performed following the procedure described by Xing et al[38]. This procedure consists of depositing Pt nanoparticles over the material of choice by adding a precursor, K_2PtCl_4. The procedure begins by depositing 15 mL of an aqueous solution containing ethylene glycol (2:1 ethylene glycol:water, volume ratio) to an aqueous solution of graphene oxide prepared following the procedure reported by Gorchinskiy et al.[39]. The resulting solution was then transferred to a volumetric flask. Then, 10 µl of K_2PtCl_4 that was previously dissolved in water at a concentration of 0.01 mol L^{-1} was deposited. To deposit Pt nanoparticles over graphene oxide sheets, the system was refluxed for 2 h using a thermostatic silicone oil bath (125 ºC). Following this step, Pt nanoparticles were deposited onto the graphene oxide sheets at a concentration of 1% by weight (with respect to rGO). Pt/graphene oxide samples were separated from the ethylene glycol solution using distilled water (washing steps) and centrifugation for three times. To complete the reduction of graphene oxide, small amounts (drops) of hydrazine hydrate were added to this solution under stirring to provide reduced graphene oxide (rGO) decorated with Pt nanoparticles [40]. The same procedure was used for depositing Pt nanoparticles over TiO_2/CdS to obtain the TiO_2/CdS/Pt nanocomposite. The samples were characterized using XRD, SEM and HR-TEM.

2.3. Preparation of quaternary nanocomposite TiO_2/CdS/rGO/Pt

Nanocomposites were prepared by dispersing 1% by weight of rGO/Pt and TiO_2/CdS into an isopropanol/water solution (2:1). The system was kept in an ultrasonic bath for 30 minutes to completely disperse the components in the solvent mixture. Afterwards, the suspension of the quaternary nanocomposite was deposited by the doctor blading technique onto an FTO substrate (active area of 2 cm^2) and then dried in an oven to evaporate the solvent to obtain TiO_2/CdS/rGO/Pt (film thickness: 6 µm). For comparison, TiO_2, TiO_2/CdS and TiO_2/CdS/Pt films were prepared using the same procedure described above for the preparation of the TiO_2/CdS/rGO/Pt nanocomposite. The nanocomposites were characterized using SEM and diffuse reflectance spectroscopy with a Varian Cary 5G UV-VIS spectrometer (NIR) equipped with a diffuse reflectance accessory.

2.4. Photocatalytic reduction of CO_2

The photoreactor was constructed by taking into account some features described in the literature[41]. It was equipped with rubber septa for collecting gaseous samples, inlet and outlet gas valves, a pressure gauge and a quartz window for sunlight illumination. The quaternary and other nanocomposites, as well as the individual samples, were deposited onto a glass substrate and then introduced inside the reactor. The system was sealed by a metal lid and nitrile rubber, specifically designed for this task. Dynamic vacuum was applied to the reactor for 30 minutes to remove air. Then, 0.5 mL of liquid water and CO_2 (99.9% purity) were injected into the reactor until a pressure of 0.2 bar was reached. The reactor was subsequently continuously illuminated by polychromatic light (AM 1.5, 100 mW cm^{-2}) for 5 h using a solar simulator (Solsim). During the illumination, the gaseous samples that formed inside the reactor were collected each hour, injected into an HP5890 series II gas chromatograph, and quantified.

2.5. Photoelectrochemical measurements

The photoelectrochemical experiments were conducted using an Autolab® PGSTAT10 potentiostat/galvanostat (Eco Chemie) controlled by GPES software, which was used for acquiring and analysing the data. A conventional three-electrode photoelectrochemical cell, consisting of the FTO/ TiO_2/CdS/rGO/Pt, FTO/TiO_2/CdS/Pt, FTO/TiO_2/CdS and FTO/TiO_2 films as working electrodes (active area of 1 cm^2); Ag/AgCl in a KCl solution (3.0 mol L^{-1}) as the reference electrode; and platinum wire as the counter electrode, was used in the experiments. An aqueous solution of Na_2SO_3 (1.0 mol L^{-1}) was used as the supporting electrolyte and sacrificial reagent (hole scavenger) to avoid degradation of the CdS nanoparticles [42,43,44]. The photoelectrochemical cell was placed in an optical bench consisting of an OrielXe (Hg) 250 W lamp coupled to an AM 1.5 filter (Oriel), collimating lenses and a water filter (Oriel). The light intensity was calibrated using an optical power metre, model 1830-C (Newport) to 100 mW cm^{-2}, but no correction was made to account for reflection and transmission losses. We used the same films in the PEC studies, with the exception of those decorated with Pt nanoparticles.

3. Results and discussion

3.1. Characterization of TiO_2/CdS and TiO_2/CdS/Pt nanoparticles

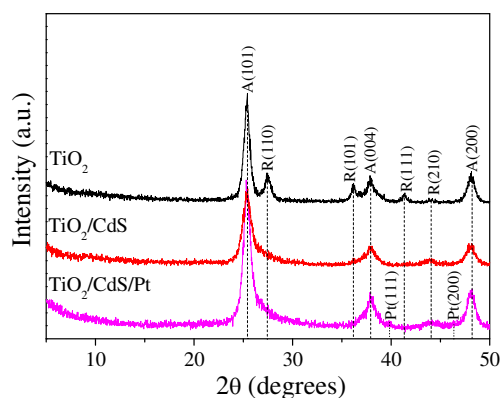Figure 1 presents powder XRD patterns of the pristine TiO_2, TiO_2/CdS and TiO_2/CdS/Pt samples.

Anatase and rutile are the crystalline phases in the pristine TiO_2 sample according to the XRD pattern shown in Figure 1. This mixture of crystalline phases has previously been reported for TiO_2 samples synthesized using other methods[45-47]. The peaks at 2θ values of 25.3°, 37.9° and 48.2° can be indexed to the (101), (004) and (200) planes of anatase titania, and the peaks at 2θ values of 27.5°, 36.2°, 41.3° and 44.1° can be indexed to the (110), (101), (111) and (210) planes of rutile titania, respectively. The powder XRD pattern of TiO_2/CdS shows broad and intense signals within the ranges of 24-30º, 35-40º and 45-50 [47-48]. These diffraction signals correspond to the crystalline planes of CdS nanoparticles, which overlapped with the diffraction peaks of anatase TiO_2. The broadening of the basal peak at 25º and increase in intensity of the peak at 44º indicate the presence of the CdS nanoparticles, which were also observed by other techniques, as discussed in the next section. Another important observation is that the characteristic XRD signals from the rutile phase observed in the XRD pattern of the pristine TiO_2 sample essentially disappear in the TiO_2/CdS sample. This result is likely a consequence of the synthesis of CdS nanoparticles in conjunction with TiO_2, which primarily contributes to the formation of anatase TiO_2 nanoparticles. The anatase crystalline phase has provided better results when applied in dye-sensitized solar cells and in other photocatalytic systems than the rutile phase[49-51]. As shown in Figure 1, it is not possible to observe the X-ray diffraction signals from platinum nanoparticles in the TiO_2/CdS/Pt systems because of the amount of platinum nanoparticles is below the detection limit of the instrument. Additional information regarding the composition of the nanocomposites was obtained by Raman spectroscopy and high-resolution microscopy (HR-TEM).

Figure 2 (a) presents the Raman spectrum of the TiO_2/CdS sample measured under a laser excitation of 514.5 nm (E_{laser} = 2.41 eV), and Figure 2 (b) shows the HR-TEM image of the TiO_2/CdS sample deposited on a copper grid. The Secondary Electron (SE) images of TiO_2/CdS nancomposite show that the two nanoparticles coexist in an aggregated form and this morphology was also confirmed by High Angle Annular Dark Field (HAADF) Images (Figure S1).
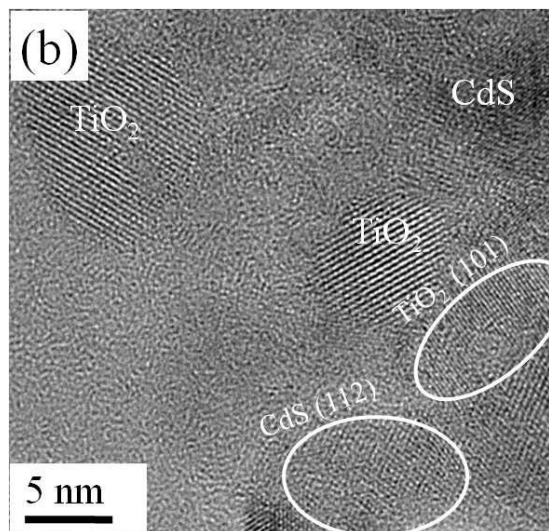

Figure 1 – Powder XRD patterns of the TiO_2, TiO_2/CdS and TiO_2/CdS/Pt samples.
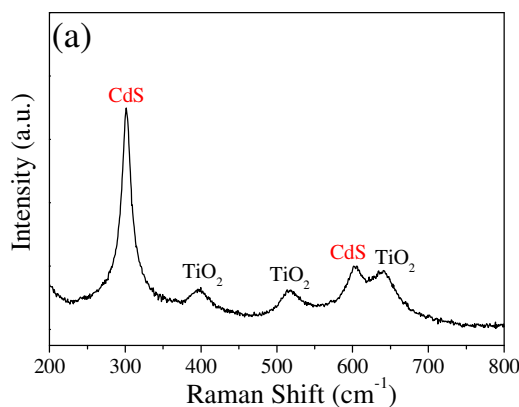
Figure 2 – (a) Raman spectrum of the TiO₂/CdS sample within the range 200-800 cm⁻¹ excited at 514.5 nm (E_laser = 2.41 eV) and (b) HR-TEM image of the TiO₂/CdS sample.

An intense resonance effect is expected for the CdS crystalline phase because the band gap of the CdS nanoparticles is 2.4 eV, which is similar to the laser excitation used to characterize the semiconductor samples in this work. This effect is indeed observed, as shown in Figure 2 (a), because an intense signal was registered at 300 cm⁻¹ and corresponds to the first-order longitudinal optical phonon (1 LO), [52]. The second-order LO is less intense, and it was registered at 600 cm⁻¹, in good agreement with results reported elsewhere for samples containing CdS [53-55]. The presence of titanium dioxide nanoparticles was also confirmed by Raman spectroscopy, as shown in Figure 2 (a), by the presence of vibrational modes at 395, 516 and 637 cm⁻¹. These signals correspond to the anatase crystalline phase of titanium dioxide [52]. Note that the characteristic Raman signals from the rutile phase were not identified because they should appear within the range of 420 to 450 cm⁻¹ [52]. This result is consistent with the data obtained from the powder XRD patterns, in which no diffraction peaks associated with the rutile phase could be identified in the TiO₂/CdS samples. Figure 2 (b) shows the HR-TEM image of this sample, where it is possible to observe the presence of CdS and TiO₂ particles. The (101) plane of TiO₂ and the (112) plane of CdS were also identified. Note that in this image, the sample is composed of nanosized spherical particles and oblate spheroids for both TiO₂ and CdS. The morphology observed in this work was also reported by other authors for a system composed of TiO₂/CdS[56].

3.2. Characterization of reduced graphene oxide decorated with platinum (rGO/Pt)

Figure 3 presents powder XRD patterns of the graphene oxide samples reduced by hydrazine and of the reduced graphene oxide decorated with Pt nanoparticles. Note that the process for depositing Pt nanoparticles over the carbonaceous material also reduces the graphene oxide sheets, giving rise to a rGO/Pt nanocomposite, a conductive material. Figure 3 also shows the thin-film XRD pattern of a Pt film on a conducting glass substrate for comparison.
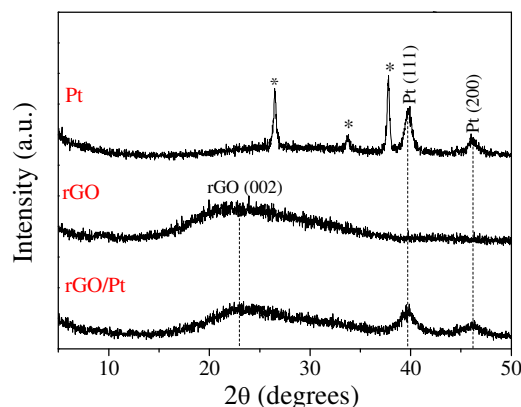

Figure 3 – Thin-film XRD pattern of a platinum film over a conducting glass substrate (Pt), powder XRD patterns of hydrazine-reduced graphene oxide (rGO) and reduced graphene oxide decorated with Pt nanoparticles (rGO/Pt).

As observed in Figure 3, graphene oxide samples reduced by hydrate hydrazine (rGO) show a broad signal with maximum intensity at 24.2°, which corresponds to an interplanar distance of d(002) = 0.37 nm, providing evidence for the loss of some oxygen-containing functional groups [57]. A similar signal profile is also observed in the graphene oxide samples decorated with Pt nanoparticles (rGO/Pt), except for the appearance of two new intense signals at 39° and 46°, which correspond to the crystalline planes of Pt with (111) and (200) orientations, respectively[57]. These two signals may be visualized in Figure 3 for the platinum film over a conducting glass substrate (Pt), thus confirming the existence of crystalline platinum. Other diffraction peaks correspond to the crystalline phases of the FTO conductive substrate, and these peaks are marked with asterisks. Xing et al. [38] also observed similar XRD patterns for carbon nanotubes decorated with Pt nanoparticles. The SEM images in Figure 4 (a) indicate that Pt nanoparticles are homogeneously dispersed over the sheets of carbonaceous material. Pt nanoparticles supported on graphene images were also observed by HAADF detector. Both aggregated and isolated Pt nanoparticles were found and the average size is around 3-4 nm (Figures 2S and 3S). It is interesting to observe that Pt nanoparticles were found in both sides of the graphene sheets as revealed by the HAADF images and their corresponding SE images.
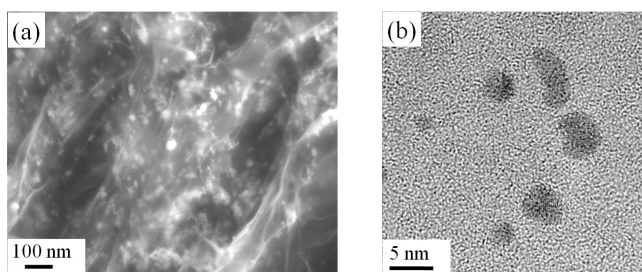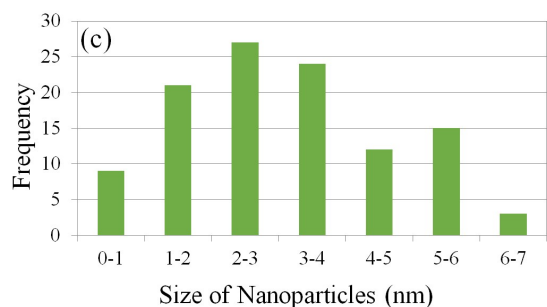
Figure 4 – (a) SEM image of rGO/Pt samples and (b) HR-TEM image of a carbonaceous material decorated with Pt nanoparticles. (c) Particle size distribution for Pt nanoparticles determined from HR-TEM images (average particle size: 3.44 nm ± 1.26).

The HR-TEM image in Figure 4 (b) shows that the Pt nanoparticles that decorate the rGO sheets have different nanoparticle morphologies and minimum aggregation. This low degree of aggregation among Pt nanoparticles provides evidence for an intense interaction between rGO sheets and the nanoparticles. Moreover, sheets from this material have a high surface area, allowing Pt nanoparticles to deposit onto both sides of the sheets, which might favour the photocatalytic processes[58,59]. Figure 4 (c) shows the particle size distribution for Pt nanoparticles determined from HR-TEM images. The Pt nanoparticles have a broad size distribution, as shown in the histogram of Figure 4 (c), with an average particle size of 3.44 nm ± 1.26. This broad particle size distribution for Pt nanoparticles is associated with the employed synthesis method, and it has already been reported elsewhere [38].

3.3. Characterization of TiO$_2$/CdS/rGO/Pt quaternary nanocomposite

The surface morphology of the TiO$_2$/CdS/rGO/Pt quaternary nanocomposite was investigated by SEM images as shown in Figure 5.

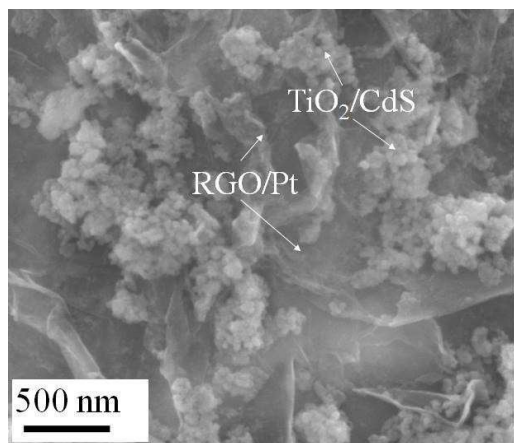**Figure 5** – SEM image of the TiO$_2$/CdS/rGO/Pt quaternary nanocomposite.

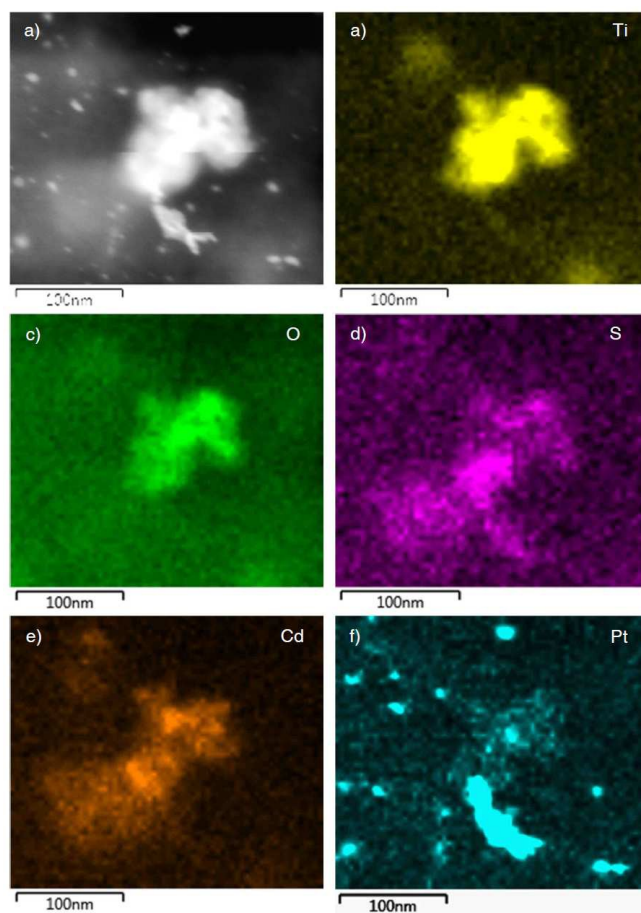**Figure 6** - EDS analyses of TiO$_2$/CdS/Pt nanoparticles on reduced graphene oxide (rGO): a) HHADF image, b) Titanium map, c) Oxygen map, d) Sulfur map, e) Cadmium map and f) Platinum map.

As shown in Figure 5, TiO$_2$/CdS nanoparticles were deposited over the rGO/Pt sheets, which have a wrinkle-paper-like surface. The TiO$_2$/CdS and Pt nanoparticles have a large dispersion over the entire rGO sheet, and this feature can positively contribute to the photocatalytic processes. The secondary electron (SE) and the high angle annular dark field (HAADF) images of the TiO$_2$/CdS/rGO/Pt quaternary nanocomposite also confirmed that both Pt and TiO$_2$/CdS nanoparticles are supported on the reduced graphene oxide layer. In addition, the Pt and the TiO$_2$/CdS nanoparticles are in both (upper and bottom) sides of graphene sheets (Figure 4S).

In order to obtain a more detailed morphology of the nanocomposite, EDS analysis was carried out in the TiO$_2$/CdS/rGO/Pt quaternary nanocomposite (Figure 6). The mapping of the elements confirms the presence of all components distributed over the graphene sheets in an intimate contact which is important for the success of the photocatalytic reaction as depicted in Figure 9.

The absorption spectra of the TiO$_2$, TiO$_2$/CdS and TiO$_2$/CdS/rGO/Pt samples were measured using diffuse reflectance spectroscopy (Figure 7).
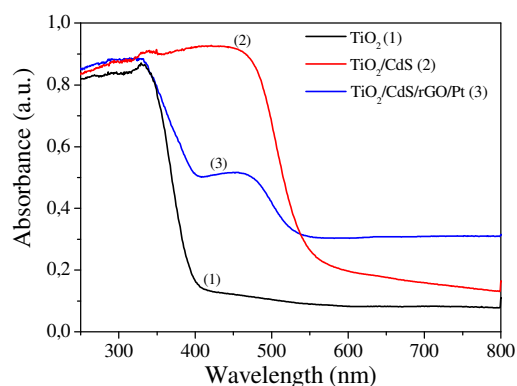
RSC Advances Accepted Manuscript

Figure 7 – Diffuse reflectance spectra of the TiO_2 (1), TiO_2/CdS (2) and TiO_2/CdS/rGO/Pt (3) nanocomposites.

The absorption of the TiO_2 nanoparticles is limited to the UV region, whereas the TiO_2/CdS sample presents a broad band from 200 to 600 nm, which is characteristic of the titania nanoparticles and of the first excitonic peak of the CdS nanoparticles [60]. Compared to the TiO_2/CdS sample, the increase in optical absorption above 400 nm for the TiO_2/CdS/rGO/Pt nanocomposite is a result of both reduced graphene oxide absorption and light scattering.

3.4. Analysis of hydrocarbon production and photoelectrochemical measurements.

The TiO_2/CdS/rGO/Pt quaternary nanocomposite was analysed as a photocatalyst for the reduction of carbon dioxide to methane in the presence of only water and solar irradiation. Figure 8 shows the results of methane production as a function of reaction time (5 h) for the quaternary nanocomposite photocatalyst and for the TiO_2, TiO_2/CdS and TiO_2/CdS/Pt samples.
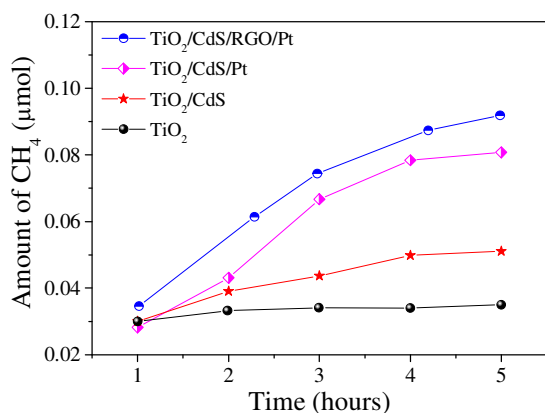

Figure 8 – Amount of methane produced by the photocatalyzis reaction in the presence of water and carbon dioxide for different samples: TiO_2, TiO_2/CdS, TiO_2/CdS/Pt and TiO_2/CdS/rGO/Pt. Reaction parameters: 50 mg of photocatalyst, CO_2 pressure inside the reactor equal to 0.2 bar, 0.5 mL of water, and illumination (100 mWcm^{-2}) for 5 h.

As shown in Figure 8, the pristine TiO_2 sample exhibits limited photocatalytic activity, giving rise to only 0.04 µmol of methane. This effect is likely a consequence of the band gap of TiO_2 (3.2 eV), with maximum absorption in the UV range, thus limiting methane production in the visible range. Wang et al. [61] achieved 0.07 µmol of methane from a TiO_2 (Degussa P25) sample using a

similar experimental procedure to that reported herein. Figure 7 also shows the production of CH_4 for the TiO_2/CdS sample, indicating a slight increase in the production of methane compared to pristine TiO_2 due to the CdS absorption in the visible range (see UV-vis spectra in Figure 6). When the TiO_2/CdS/rGO/Pt nanocomposite containing graphene sheets decorated with Pt nanoparticles was employed, the production of methane significantly increased, even compared to Pt-coated TiO_2/CdS samples. This effect results from the beneficial synergy between all four components in the photogeneration, charge separation and transport of the charge carriers.

The mechanism involved in the production of methane from CO_2 and water is complex and begins upon photoexcitation of the two semiconductors. First, it is interesting to consider the energy level diagram of all components in the TiO_2/CdS/rGO/Pt quaternary nanocomposite. The relative energetic positions of the conduction band (CB), valence band (VB) and work function (Φ) for TiO_2, CdS, RGO and Pt are shown in Figure 8 (a). A schematic illustration of the photoinduced charge separation and transfer process in the TiO_2/CdS/rGO/Pt quaternary nanocomposite is also presented in Figure 8 (b).
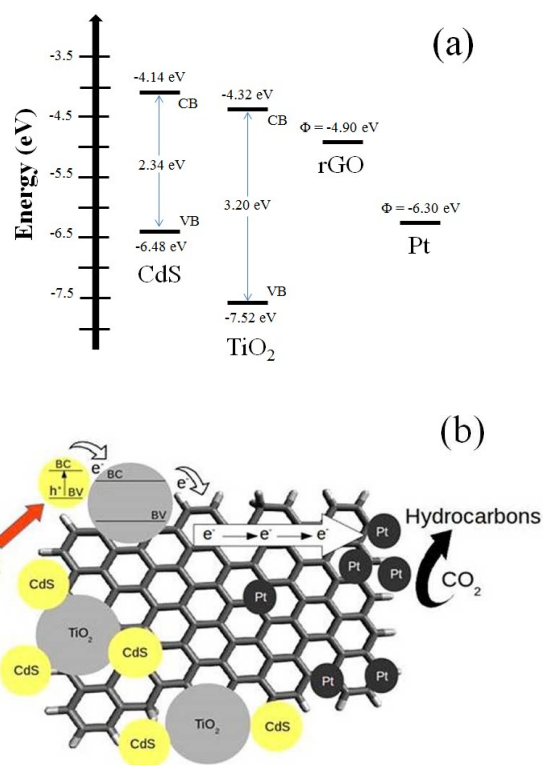

Figure 9 – (a) Energy level diagrams for TiO_2, CdS, RGO and Pt. CB, VB and Φ are the conduction band, valence band and work function, respectively. (b) Schematic illustration of the photoinduced charge separation and transfer process in the TiO_2/CdS/rGO/Pt quaternary nanocomposite.

As shown in Figure 9 (a), the energies of the TiO_2 CB and VB are -4.32 and -7.52 eV, respectively, whereas those for the CdS on TiO_2 are -4.14 and -6.48 eV[62], respectively. In addition, the ϕ of rGO and Pt are approximately -4.9 eV and -6.3 eV, respectively[63,64] In this diagram, the CB edge of CdS is above that of TiO_2. When the TiO_2/CdS/rGO/Pt nanocomposite is exposed to visible light, excited electron–hole pairs are generated in both semiconductors. Due to the

specific nature of the band alignment at the TiO_2/CdS interface, the photogenerated electrons are transferred to the CB of TiO_2, whereas the holes remain in the VB of CdS.[65,66, 67] The spatial separation of the photogenerated electron-hole pairs in different semiconductors reduces charge recombination and is important for photocatalyzis and photoelectrochemical devices[68,69]. The rGO sheets are a well-known electron-accepting material with excellent conductivity properties as a result of its two-dimensional planar structure. Thus, a faster electron transfer from both TiO_2 and CdS nanomaterials to the rGO sheets (via the titania conduction band) is expected to occur. The rapid transport of the charge carriers in the graphene sheets promotes an even better charge separation. This process eventually decreases the rate of recombination of the photogenerated electron-hole pairs.

In addition, the high surface area provided by the carbonaceous material favoured a homogeneous distribution of the Pt nanoparticles and a strong physical contact between the TiO_2 and CdS nanoparticles. In this respect, the Pt nanoparticle co-catalyst also efficiently contributes to conduct electrons towards carbon dioxide molecules, thereby reducing them to methane. Figure 8 (b) schematically illustrates how the proposed photoinduced charge separation and transfer process occurs in the TiO_2/CdS/rGO/Pt quaternary nanocomposite.

According to Inoue et al.[70], the conversion of CO_2 to methane involves a multistep reduction process given by:

$$H_2O_{(l)} + 2\ h^+ \rightarrow ½O_{2(g)} + 2H^+_{(aq)} \qquad \text{Eq. 1}$$
$$CO_{2(aq)} + 2H^+_{(aq)} + 2e^- \rightarrow HCOOH \qquad \text{Eq. 2}$$
$$HCOOH + 2H^+_{(aq)} + 2e^- \rightarrow HCHO + H_2O_{(l)} \qquad \text{Eq. 3}$$
$$HCHO + 2H^+_{(aq)} + 2e^- \rightarrow CH_3OH \qquad \text{Eq. 4}$$
$$CH_3OH + 2H^+_{(aq)} + 2e^- \rightarrow CH_4 + H_2O_{(l)} \qquad \text{Eq. 5}$$
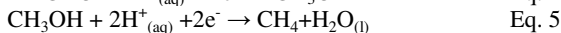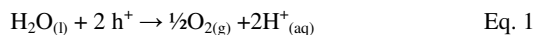
where e^- and h^+ denote photogenerated electrons and holes, respectively. First, the presence of h^+ promotes water splitting, resulting in the formation of oxygen gas (O_2) and H^+ ions. These H^+ ions, when combined with CO_2 molecules and electrons, promote the formation of organic molecules (hydrocarbons), which at the end of the process are converted to methane by adding more protons and electrons[71].

In summary, the photocatalytic results indicate that the TiO_2/CdS/rGO/Pt quaternary nanocomposite exhibited better performance towards CO_2 photoreduction than the TiO_2, TiO_2/CdS and TiO_2/CdS/Pt nanocomposites. This conclusion is also supported by the photoelectrochemical measurements performed using the TiO_2/CdS/rGO/Pt quaternary nanocomposite and using the TiO_2, TiO_2/CdS and TiO_2/CdS/Pt films deposited onto FTO substrates (Figure 9). The substrates were employed as working electrodes in a typical three-electrode photoelectrochemical cell.
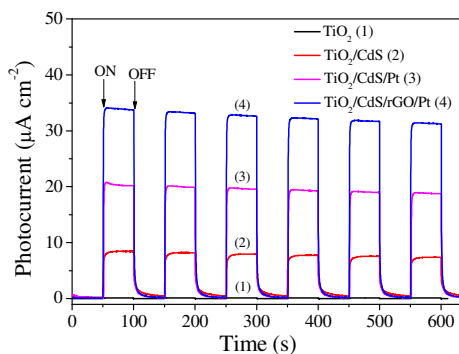

Figure 10 – Time-dependent photocurrent density (chronoamperometry) at 0 V versus Ag/AgCl applied bias potential in an aqueous electrolyte containing 1 mol L^{-1} Na_2SO_3 and using the TiO_2 (1), TiO_2/CdS (2), TiO_2/CdS/Pt (3) and TiO_2/CdS/rGO/Pt (4) films on an FTO substrate as the working electrode.

As observed in the chronoamperometry measurements (Figure 10), the photocurrents responded immediately to the presence of light when the cell operation was interrupted every minute for 50 s (on/off cycle). All samples exhibited anodic photocurrent, indicating that the electron flux is towards the electrode and then driven to the platinum wire by the external circuit. The films prepared with TiO_2 nanoparticles showed only a small photoactivity, i.e., a low photocurrent due to its limited band gap in the ultraviolet region[72]. For the TiO_2/CdS film, appreciable values of photocurrent appeared immediately under illumination (ON) and decreased to nearly zero in dark conditions (light OFF). This effect is due to a strong absorption of CdS nanoparticles in the visible region, followed by a fast electron transfer to the TiO_2 nanoparticles[62,63]. An enhancement in the anodic photocurrent values was observed for the TiO_2/CdS/rGO/Pt nanocomposite compared to TiO_2/CdS/Pt and TiO_2/CdS. In fact, platinum nanoparticles contribute to the increase in the photocatalytic activity of the systems, as previously reported [73,74]. The higher anodic current for the TiO_2/CdS/rGO/Pt nanocomposite is consistent with the photocatalyzis data as a higher amount of methane gas was detected when the TiO_2/CdS/rGO/Pt nanocomposite was employed, suggesting that the quaternary nanocomposite is an efficient material for photocatalyzis. It is difficult to quantitatively evaluate the contribution of each component separately. We strongly believe that electrons are transported more efficiently through the RGO sheets, thereby decreasing the recombination between electrons in the TiO_2 CB and the holes in the CdS VB. In addition, the presence of Pt nanoparticles is important for more efficiently catalyzing the CO_2 reduction reaction. Coupling two semiconductors (TiO_2 and CdS) with complementary absorption profiles and suitable energy levels, which allowed an efficient electron transfer between them, was also a key factor for the success of this quaternary nanocomposite.

4. Conclusions

TiO_2/CdS and rGO/Pt nanocomposites were synthesized separately and then mixed to obtain a new TiO_2/CdS/rGO/Pt nanocomposite with interesting properties for application in photocatalyzis. The XRD data indicated that anatase was the main crystalline phase in pristine TiO_2, likely due to the simultaneous synthesis of CdS in conjunction with TiO_2. According to the SEM and HR-TEM images, Pt nanoparticles deposited over rGO sheets are homogeneously dispersed over the entire sheet of carbonaceous material. The TiO_2/CdS/rGO/Pt nanocomposite was investigated as a photocatalyst for the reduction of carbon dioxide to methane in the presence of only water and visible light. The TiO_2/CdS/rGO/Pt nanocomposite provided higher photocatalytic activity than TiO_2, TiO_2/CdS and TiO_2/CdS/Pt samples. This result suggests that the transport of photogenerated charges occurs in the carbonaceous material, which is favoured by the relatively high rGO surface area, by the efficient contact among TiO_2/CdS nanoparticles and by the presence of Pt nanoparticles, which are able to efficiently transport electrons towards carbon dioxide molecules. The enhanced electron transport in the graphene films of TiO_2/CdS/rGO/Pt nanocomposite was also evidenced in the photoelectrochemical measurements.

5. Acknowledgements

the LNNano (Laboratório Nacional de Nanotecnologia) in Campinas, Brazil.

6. References

[1] M. Mikkelsen, M. Jorgensen, F. C. Krebs, *Energy Environ. Sci.,* 2010, 3, 43 –81.

[2] K. Mori, H. Yamashita, M. Anpo, *RSC Adv*., 2012, 2, 3165–3172.

[3] M. Anpo, H. Yamashita, *In Heterogeneous Photocatalysts; M. Schiavello.*, Ed; John Wiley & Sons., Chichester, 1997, 133–168.

[4] T. Inoue, A. Fujishima, S. Konishi, K. Honda, *Nature*, 1979, 277,637–640.

[5] M. Anpo and K. Chiba, *J. Mol. Catal*., 1992, 74, 207–302.

[6] M. Halmann, *In Energy Resources through Photochemistry and Catalysis.*, 1983, 507–565.

[7] J.Ma, N.Sun, X.Zhang, N.Zhao, F.Xiao, W.Wei, Y.Sun, *Catalysis Today.*, 2009, 148, 221–231.

[8] H-ah. Park, J. H. Choi, K. M. Choi, D. K. Lee, J. K. Kang, *J. Mater. Chem.*, 2012, **22**, 5304-5307.

[9] S. C. Roy, O. K. Varghese, M. Paulose, C. A. Grimes, *ACS Nano.*, 2010, 4, 1259–1278.

[10] M. Jitaru, D. A. Lowy, M. Toma, B. C. Toma, L. Oniciu, J. of Applied Electrochemistry., 1997, 27. 875-889.

[*11*] *N. V. Rees, R. G. Compton,* Energy Environ. Sci., *2011, 4, 403-408.*

[12] J. Núñez, V. A. de la Peña, O'Sheaa, P. Janaa, J. M. Coronadoa, D. P. Serranoa, *Catalysis Today.*, 2013, 209, 21–27.

[13] S. C. Roy, O. K. Varguese, M. Paulose, C. A. Grimes, *ACS Nano,* 2010, 4, 1259-1278.

[14] T. Inoue, A. Fujishima, S. Konishi, K. Honda, *Nature*., 1979, 277, 637-638.

[15] K. Hashimoto, H. Irie, A Fujishima, *Japanese J. Appl. Phys.,* 2005, 44, 8269-8285.

[16] Y. Bessekhouad, Y, D. Robert, J. V. Weber, *J. Photochem. Photobiol. A.,* 2004, 163, 569–580.

[17] N. Serpone, P. Marathamuthu, P. Pichat, E. Pelizzetti, H. Hidaka, *J. Photochem. Photobiol., 1995,* 85, 247–255.

[18] S. Qian, C Wang, W. Liu, Y. Zhu, W. Yao, X. Lu, *J. Mater. Chem.*, 2011, 21, 4945-4952.

[19] E. A. Koslova, N. S. Kozhevnikova, S. V. Cherepanovaa, T. P. Lyubina, E. Y. Gerasimov, V. V. Kaichev, A. V. Vorontsov, S. V Tsybulya, A. A. Rempel, V. N. Parmon, *Journal of Photochemistry and Photobiology A: Chemistry*., 2012, 250, 103– 109.

[20] H. Zhang, Y. Zhu, *J. Phys. Chem. C.,* 2010, 114, 5822-5826.

[21] C. Wang, R. L. Thompson, J. Baltrus, C. Matranga, *J. Phys. Chem. Lett.* 2010, 1, 48-53.

[22] K. Maeda, K. Teramura, D. L. Lu, T. Takata, N. Saito, Y. Inoue, K. Domen, *Nature.,* 2006, 440, 295.

[23] J. Tang, A. J. Cowan, J. R. Durrant, K. R. David, *J. Phys. Chem. C* 2011, 115, 3143-3150.

[24] A. J. Cowan, J. Tang, W. Leng, J. R. Durrant, D. R. Klug, *J. Phys. Chem. C.,* 2010, *114,* 4208-4214

[25] B. O'Reagan, J. Moser, M. Anderson, M. Grätzel, *J. Phys. Chem.,* 1990, 94, 8720-8726.

[26] H. Rensmo, K. Keis, H. Lindström, S. Södergren, A. Solbrand, A. Hagfeldt, S.-E. Lindquist, L. N. Wang, M. Muhammed, *J. Phys. Chem. B*., 1997, 101, 2598-2601.

[27] X-H. Xia, Z-J. Jia, Y. Yu, Y. Liang, Z. Wang, L-L. Ma, *Carbon* 2007, 45, 717-721.

[28] A. Morais, L. M. D. Loiola, J. E. Benedetti, A. S. Golçalves, C. A. O. Avellaneda, J. H. Clerici, M.A. Cotta, A. F. Nogueira, *J. Photochem. Photobiol. A: Chem.*, 2013, 251, 78-84.

[29] J. Wanga, P. Yanga, J. Zhaoa, Z. Zhua, *Appl. Surface Sci., 2013, 282, 930-936.*

[30] C. H. Kim, B-H. Kim, K. S. Yang. *Carbon.,* 2012, 50, 2472-2481.

[31] S. B, X. Shen, H. Lv, G. Zhu, C. Bao, Y. Shan, *J. Colloid Interface Sci.,* 2013, 405, 1–9.

[32] S. N. Habisreutinger, L. S-Mende, J. K. Stolarczyk, *Angew. Chem. Int. Ed*.,2013, 52, 7372 – 7408.

[33] M. Gatrell, N. Gupta, A. Co, *J. Electroanal. Chem.,* 2006, *594,* 1–19.

[34] Liu, Y., Li, D. G. and Sun, S. S, *J. Mater. Chem*., 2011, 21, 12579-12587.

[35] Doner, A., Taskesen, E. and Kardas, G, *Int J. Hyd Energy*., 2014, 39, 11355-11359.

[36] Cheng, J., Zhang, M., Wu, G., Wang, X., Zhou, J. H. and Cen, K. F, *Sol. Energ. Mat. Sol. C.*, 2015, 132, 606-614.

[37] G. S. Li, D. Q. Zang, J. yu, C.; *Environ. Sci. Technol.,* 2009, 43, 7079-7085.

[38] Y. Xing, *J. Phys. Chem. B.,* 2004, 108, 19255-19259.

[39] N. I. Kovtyukhova, P.J. Ollivier, B. R. Martin, T. E. Mallouk, A. S. Chizhik, E. V. Buzaneva, A. D. Gorchinskiy, *Chem. Mater.,* 1999, 11, 771-778.

[40] D. Li, M. B. Muller, S. Gilje, R. B. Kaner, G. G. Wallage, *Nature Nanotechnol.,* 2008, 3, 101-105.

[41] O. K. Varghese, M. Paulose, T. J. Latempa, G. A. Grimes, *Nano Lett.*, 2009, 9, 731-737.

[42] Zhang, Q., Wang, L., Feng, J. T., Xu, H. and Yan, W, *Phys. Chem. Chem. Phys.*, 2014, 16, 23431-23439.

[43] Luo, J. S., Ma, L., He, T. C., Ng, C. F., Wang, S. J., Sun, H. D. and Fan, H. J. TiO2/(CdS, CdSe, CdSeS), *J. Phy. Chem. C.*, 2012, 116, 11956-11963.

[44]] Wang, H. Y., Wang, G. M., Ling, Y. C., Lepert, M., Wang, C. C., Zhang, J. Z. and Li, Y, *Nanoscale.* 2012, 4, 1463-1466.

[45] S.V. Cherepanova, *J. Struct. Chem.,* 2012, 53, 113–136.

[46] T. Lv, L. Pan, X. Liu, Z. Sun, *Electrochim. Acta.*, 2012, 83, 216– 220.

[47] J. Kim, H. Choi, C. Nahm, C. Kim, S. Nam, S. Kang, D-R. Jung, J. I. Kim, J. Kang, B. Park, *J. Power Sources.*, 2012, 220,108-113.

[48] A. A. Rempel, A. Magerl, *Acta Crystallographica A.,* 2010, 66, 479–483.

[49] T. Hirakawa, K. Yawata, Y. Nosaka, *Appl. Catal. A.,* 2007, 325, 105.

[50] A. Sclafani, J. M. J. Herrmann, *Phys. Chem.,* 1996, 100, 13655.

[51] Y. Yamada, Y. Kanemitsu, *Appl. Phys. Lett.,* 2012, 101, 133907.

[52] J. C. Tristão, F. Magalhães, P. Coriob, M. T. C. Sansiviero, *J. Photochem. Photobiol. A: Chem.,* 2006, 181, 152–157.

[53] J.M. Nel, H.L. Gaigher, F.D. Auret, *Thin Solid Films* 436 (2003)186–195.

[54] B. Schreder, C. Dem, M. Schmitt, A. Materny, W. Kiefer, U. Winkler, E. Umbach, *J. Raman Spectrosc.,* 2003, 34, 100–1003.

[55] A. Gichuhi, B. E. Boone, C. J. Shannon, *Electroanal. Chem.,* 2002, 522, 21–25.

[56] E. A. Kozlova, N.S. Kozhevnikova, S. V. Cherepanova, T. P. Lyubina, E. Y. Gerasimov, V.V. Kaichev, A. V. Vorontsov, S. V. Tsybulya, A. A. Rempel, V. N. Parmon, *J. Photochem. Photobiol A: Chem.,* 2012, 250, 103–109.

[57] M-Y. Yen, C-C. Teng, M-C. Hsiao, P-I. Liu, W-P. Chuang, C-C. M. Ma, C-K. Hsieh, M-C. Tasib, C-H. Tsaib, *J. Mater. Chem.,* 2011, 21, 12880–12888.

[58] Y. C. Si, E. T. Samulski, *Chem. Mater.,* 2008, 20 -21 6792–6797.

[59] C. Xu, X. Wang, J. W. Zhu, *J Phys Chem., C* 112 2008, 50, 19841–19845.

[60] Y. Bessekhouad, N. Chaoui, M. Trzpi, N. Chazzal, D. Robert, J. V. Weber, *J. Photochem. Photobiol. A: Chem.,* 2006, 183, 218–224.

[61] S. Xie, Y. Wang, Q. Zhang, W. Fan, W. Deng, Y. Wang, *Chem. Commun.*, 2013, 49, 2451.

[62] C-F. Chi, H-W. Cho, H. Teng, C-Y. Chuang, Y-M-Chang, Y-J. Hsu, Y-L. lee, *Appl. Phys. Lett*., 2011, 98, 012101.

[63] B. Kang, S. Lim, W. H. Lee, S. B. Jo, K. Cho, *Adv. Mater*., 2013, 25, 5856-5862.

[64] X. Zhang, Yu-L. C, R-S-Liu, D-P-Tsai, *Rep. Prog. Phys,* 2013, 76, 046401.

[65] N. Serpone, P. Maruthamuthu, P. Pichat, E. Pelizzetti, H. Hidaka *J. Photochem. Photobiol. A: Chem.,* 2006, 85, 247-255.

[66] H. T, T. Mitsui, T. Kiyonaga, T. Akita, K. Tanaka, *Nature Materials.,* 2006, 5, 782 – 786.

[67] L.L. Tang, W-J Ong, S.P. Chai, *Nanoscale Res. Lett*., 2013, 8, 465.

[68] H Li, X. Zhang, D. R. MacFarlane Adv. Energy Mater. 2014, 1401077.

[69] X. An, K. Li, J. Tang ChemSusChem 2014, 7, 1086-1093.

[70] T. Inoue, A Fujishima, S. Konishi, K. Honda, P,. *Nature.* 1979, 277, 637-638.

[71] S. C.Roy, O. K. Varghese, M. Paulose, C. A. Grimes, *Acs Nano.* 2010, 4, 1259-1278.

[72] X. Liu, L. Pan, T. Lv, Z. Sun, *J. Alloys Compounds*., 2014, 583, 390-395.

[73] X.L. Fu, J.L. Long, X.X. Wang, D. Leung, Z.X. Ding, L. Wu, *J Hydrogen Energy.* 2008, 22, 6484–6491.

[74] D.I. Kondarides, V.M. Daskalaki, A. Patsoura, X.E. Verykios, *Catal Lett., 2008,* 122, 26–32.